RSC Advances

PAPER

View Article Online
View Journal | View Issue

Cite this: *RSC Adv.*, 2019, **9**, 16831

The visual detection of anesthetics in fish based on an inverse opal photonic crystal sensor†

Shili Chen,[a] Hui Sun,*[ac] Zhenjian Huang,[a] Zhenkai Jin,[a] Siyang Fang,[a] Jiahua He,[a] Yangyang Liu,[a] Yi Zhang[a] and Jiaping Lai*[b]

Received 3rd March 2019
Accepted 10th May 2019

DOI: 10.1039/c9ra01600g

rsc.li/rsc-advances

A novel smart sensor for the rapid and label-free detection of benzocaine has been developed based on the combination of photonic crystal (PC) and molecular imprinting polymer (MIP) techniques. A molecularly imprinted photonic crystal (MIPC) hydrogel film was prepared *via* a non-covalent, self-assembly approach with a PC mould. With a highly ordered inverse opal structure, the resulting benzocaine MIPC exhibited high sensitivity, smart specificity, quick response times and good regeneration abilities. It can give rise to a readable optical signal and color change upon binding with benzocaine, with a detection limit of 16.5 μg mL^{-1}. The sensor has been successfully used to visually estimate benzocaine concentrations in fish samples. In comparison with HPLC, the developed MIPC sensor has shown satisfactory accuracy in terms of results. It has great potential for on-site screening and the visual detection of trace benzocaine in real samples.

Introduction

With the development of economies worldwide, in order to satisfy the increasing human consumption of live fish, high-density live fish transportation is becoming more and more popular. During transportation, the disturbance of the physiological and metabolic activities of fish will aggravate skin injuries and disease and even cause the death of fish. In order to improve fish survival rates, anesthetics are often applied during transportation to reduce the physiological stress response of fish.[1] However, if the dosage is excessive or the anesthesia application time is too long, the anesthetics will go deep into fish medulla, ultimately resulting in death.[2] In addition, the intake of aquatic products with excessive amounts of anesthetic will cause harm to human health. Therefore, a certain withdrawal time is needed in relation to these anesthetized fish before they are eaten. The length of the withdrawal time depends on the fish itself, the type of anesthesia and the way the anesthetic is applied. At present, there is a lack of related laws, regulations and testing standards for fish anesthetics in the market.[3,4]

In addition, anesthetic residues may spread in water and soil, giving rise to serious risks to the environment. Therefore, the evaluation and monitoring of trace levels of anesthetics are necessary to protect human health and to control environmental pollution. Various analytical methods, including liquid chromatography-mass spectrometry (LC-MS),[5] LC-MS/MS,[6] ultra-performance liquid chromatography-mass spectrometry (UPLC-MS),[7] high-performance liquid chromatography (HPLC),[8] HPLC-MS/MS,[9] solid-phase extraction (SPE),[10] gas chromatography-mass spectrometry (GC-MS),[11] capillary electrophoresis (CE),[12,13] enzyme-linked immunosorbent assays (ELISAs),[14] and so on, have been proposed for the determination of anesthetics in various types of samples. Although all of these methods have shown sensitivity and specificity for the detection of anesthetics, they are expensive and time-consuming, and require complicated sample pre-treatment and sophisticated equipment. All of these drawbacks limit their application to the onsite detection of anesthetics in real-life markets. As a result, considerable interest has arisen in the development of alternative cost-effective and easily handled technologies for the visual detection of anesthetics in environmental samples.

Recently, inverse opal photonic crystals (PCs) have drawn increasing attention for the purpose of the visual detection of various analytes and environmental stimuli (such as temperature, pH and humidity).[15–17] Owing to their periodic porous structures, such PC materials have unique photonic band gaps (PBGs). They can exhibit fascinating optical properties (Bragg diffraction) and bright structural colours. If the periodic spacing of the 3D-ordered skeleton is changed, a PC sensor will display an obvious color change or a shift in its diffraction spectrum. However, normal PCs lack the properties for molecular recognition, that is, any changes in environmental conditions may give rise to optical signals.

[a]*College of Environmental Science and Engineering, Guangzhou University, Guangzhou 510006, Guangdong, China. E-mail: esesunhui@gzhu.edu.cn*

[b]*Guangzhou Key Laboratory of Analytical Chemistry for Biomedicine, School of Chemistry & Environment, South China Normal University, Guangzhou 510006, Guangdong, China. E-mail: laijp@scnu.edu.cn*

[c]*Guangdong Provincial Key Laboratory of Radionuclides Pollution Control and Resources, Guangzhou 510006, Guangdong, China*

† Electronic supplementary information (ESI) available. See DOI: 10.1039/c9ra01600g

On the other hand, molecular imprinting is a well-established and facile technique used to synthesize molecularly imprinted polymers (MIPs) with specific molecular recognition nanocavities.[18–23] Owing to the complementarity of the shape and binding sites with the template molecules used, the created nanocavities can act as artificial antibodies. Possessing desirable selectivity, physical robustness and cost effectiveness, various MIPs have been developed and used for chromatographic separation, sensors, sample pre-treatment and so on. MIPs for the recognition of anesthetics have also been prepared.[24–26] However, for traditional MIPs, the molecular recognition process is not self-expressive. Unless the target has a chromophore or a fluorophore, or is electroactive, the analyte must be modified or labeled. Those types of procedures are complex. Therefore, a smart, label-free, and visual MIP sensor is preferred for fast detection.

In particular, to endow PCs with high selectivity, molecular imprinting has been explored to produce recognition sites in PCs.[27–30] Obviously, the massive macropores in molecularly imprinted photonic crystals (MIPCs) are favourable for mass transportation and fast accessibility to recognition sites. Therefore, the combination of PCs and MIPs is a promising approach to realize the visual detection of specific analytes with high sensitivity and quick response times, but without the need for labelling techniques and expensive instruments.

In the present research, we have developed a convenient and easily handled MIPC sensor with an inverted opal structure for the rapid and label-free detection of benzocaine (BZ), one of the anesthetics often used for fish anesthesia. After a series of optimizations of the polymerization method, elution time and adsorption medium, we obtained MIPC sensors with admirable sensitivity, satisfactory specificity, rapid responsiveness and excellent recoverability. The developed MIPCs can give rise to a readable optical signal upon binding with the target analytes. Compared with structurally similar compounds, the sensors exhibit high selectivity toward BZ with strong responses. The sensors have been used to visually estimate BZ concentrations in fish samples. By comparison with HPLC, the developed MIPC sensor showed satisfactory accuracy in terms of results from real sample detection.

Experimental

Materials

Tetraethyl orthosilicate (TEOS), benzocaine and procaine were purchased from Aladdin (Shanghai). 25% ammonia solution, 45% hydrofluoric acid and 30% hydrogen peroxide were purchased from Guangzhou Chemical Reagent Factory. Anhydrous ethanol, hydrochloric acid, concentrated sulfuric acid (H_2SO_4, 98%), and glacial acetic acid (H_2O_2, 30%) were purchased from Tianjin Zhiyuan Chemical Reagent Co., LTD. Ethylparaben was purchased from Tianjin Kermel Chemical Reagent Co., LTD. 2-Hydroxyisobutyric acid was purchased from Shanghai Renxi Technology Co., LTD. 2,2-Azobisisobutyronitrile (AIBN) and methacrylate acid (MAA) were purchased from Tianjin Damao Chemical Reagent Factory. Ethylene glycol dimethacrylate (EDMA) was purchased from Alfa Aesar Chemical Co., LTD. All of the above chemicals were of analytical grade.

Glass slides (76.2 × 25.4 × 1 mm) were purchased from Jiangsu Swift Boat Glass and Plastic Co., LTD. Polymethyl methacrylate (PMMA) slides (50 × 12 × 1.3 mm) were purchased from Yali Organic Process Factory. Organic microporous membranes with 0.45 μm diameter pores were purchased from Tianjin Keyilong Experimental Equipment Co., LTD.

Fabrication of the SiO_2 colloidal sol

The silica colloidal sol was fabricated *via* the hydrolysis of tetraethyl orthosilicate (TEOS) in the presence of ammonia.[31] A mixture of TEOS, ammonia, and ethanol was stirred at 500 rpm for 2 h at 30 °C, and a milk-white SiO_2 colloidal sol was obtained. The silica particles were rinsed with anhydrous ethanol five times to remove unreacted residue and they were then fully dispersed in anhydrous ethanol using an ultrasonic bath. The cleaned silica colloidal particles were stored in vials separately at different weight concentrations.

Self-assembly of the SiO_2 photonic crystal (PC) template

Photonic crystal templates were prepared from the obtained SiO_2 colloidal sol using a vertical deposition method.[32] The glass slides were cleaned and made hydrophilic by immersing them into H_2SO_4/H_2O_2 (7/3, v/v) solution for 12 h followed by rinsing with water. Then the glass slides were immersed vertically in cylindrical glass containers. At the same time, the SiO_2 colloidal sol was adjusted to 0.2 wt% and then poured into the above cylindrical glass containers. These containers were then put into a constant temperature and humidity chamber at 30 °C for 4 days while being exposed to a relative humidity of 50%. With the evaporation of the ethanol, photonic crystal templates were obtained on both sides of each glass slide.

Fabrication of MIPC films

The molecularly imprinted photonic crystal (MIPC) fabrication method is shown in Fig. 1. 0.1 mmol of the template molecule (benzocaine), 0.5 mmol of MAA (functional monomer) and 0.125 mmol of EGDMA (crosslinker) were dissolved in 200 μL of methanol. Finally, 0.003 g of AIBN (initiator) was added to the mixture for the preparation of the precursor solution. The precursor solution was then sonicated for 30 min, and then deoxygenated with nitrogen (N_2) for 5 min.

Two polymethyl methacrylate (PMMA) slides were put respectively on and under a glass slide that had been modified with the SiO_2 colloidal crystal templates. These three slides were

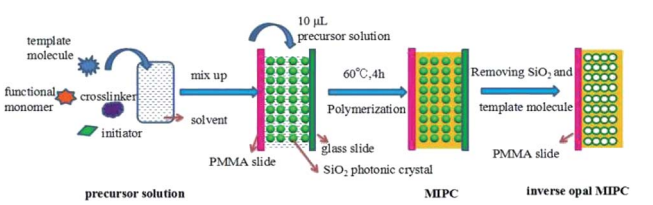

Fig. 1 The fabrication of inverse opal MIPC films.

clipped tightly together to form a "sandwich structure". Then 10 μL of precursor solution was transferred with a pipette filler into each space between the slides of the "sandwich". When the precursor solution had fully filled the voids of the colloidal crystal template, the "sandwich" became transparent. Then the "sandwich" was put into a water bath at 60 °C for 4 h for polymerization. After polymerization, the "sandwich" was soaked in hydrofluoric acid solution (4 wt%) and glacial acetic acid/methanol/water (0.5/3.5/6, v/v/v) in sequence to remove the SiO_2 templates and benzocaine (BZ), respectively. Finally, inverse opal MIPC films were obtained on both PMMA slides. Non-imprinted photonic crystals (NIPCs) were synthesized in the same manner but in the absence of BZ.

Characterization of PCs and MIPCs/NIPCs

SEM images of the PCs and inverse opal MIPC/NIPC films were obtained using a JSM-7001F field emission scanning electron microscope (Hitachi, Japan). The color changes of the silica colloidal based PC templates and MIPC films were recorded using a digital camera. The Bragg diffraction wavelength shifts of the MIPCs were recorded using an integrating sphere and a fiber-optic spectrometer (Ocean Optics, Maya 2000 PRO).

To explore the effects of different methanol content values on the optical properties of MIPCs, we changed the concentration of methanol in the methanol/water binary system from 0 to 50% (v/v), while keeping the BZ concentration at 20 mM.

To investigate the response time between the MIPC film and the substrate, we put the same piece of MIPC film in 20 mM BZ solution for different time periods and observed the diffraction peak wavelength shifts.

To make a calibration curve of the response of the MIPC to changes in the BZ content, the same piece of MIPC film was put into BZ solutions with BZ concentrations ranging from 0.1 mM to 20 mM. The Bragg diffraction wavelength shift of the MIPC was recorded using an integrating sphere and a fiber-optic spectrometer. To explore the specificity and selectivity of the MIPC, three structural analogues (2-hydroxy isobutyric acid, ethylparaben and procaine hydrochloride) were prepared with concentrations ranging from 0.1 mM to 20 mM and analyzed with MIPCs and NIPCs.

Application

Fish (grass carp, a top seller in the market) were bought from the market. After cleaning, shredding and stirring, several samples of fish (1.0000 g each) were put into 50 mL centrifuge tubes. Methanol was used to extract BZ with an ultrasonic bath. After centrifugation, the supernatant was collected and filtered through 0.45 μm pore organic microporous membranes prior to detection with the MIPCs. A Maya 2000 PRO fiber-optic spectrometer was used to determine the MIPC diffraction shifts. A camera was used to take pictures of the color changes of the MIPCs before and after immersion in fish samples.

Results and discussion

Preparation of PCs and inverted opal MIPC film

Photonic crystals (PCs) were prepared *via* the vertical deposition of colloidal silica on glass substrates. They were then used as moulds for the formation of 3D highly ordered, interconnected microporous MIPCs with an inverse opal structure. The benzocaine MIPCs were prepared *via* a non-covalent, self-assembly approach. Fig. 1 shows the processes for the preparation of benzocaine MIPCs: the preparation of the SiO_2 PC template; the polymerization of the precursor solution in the voids of the SiO_2 colloidal crystals; and the removal of the SiO_2 microspheres and benzocaine molecules.

It is known that the λ_{max} value of the Bragg diffraction peak of the resulting PCs is determined by SiO_2 particle size according to the following equation:

$$\lambda_{max} = 1.633d \times n_{eff} = 2.32d \quad (1)$$

where λ_{max} is the peak wavelength of the Bragg diffraction spectrum; d is the diameter of the SiO_2 colloidal spheres; and n_{eff} is the average effective refractive index of the PCs (for PCs with a face centred cubic (FCC) structure, $n_{eff} = 1.42$).[33,34]

Thus, the particle size and mono-dispersity of the silica spheres were firstly optimized to get ideal PCs with a suitable Bragg diffraction spectrum. According to the literature,[35,36] the shape, particle size and mono-dispersity of silica spheres are determined by the hydrolysis rate constant of TEOS. And the relationship between the hydrolysis rate constant of TEOS and the concentrations of ammonia and TEOS can be explained as follows:

$$k' = -\frac{d[TEOS]}{dt} = 15.75 \exp(-22053.9/RT)[NH_3]^{1.02}[H_2O]^{1.42}[TEOS] \quad (2)$$

where k' is the hydrolysis rate constant of TEOS; T is the temperature of the reaction system; $[NH_3]$, $[H_2O]$ and [TEOS] are the concentrations of ammonia, water and TEOS, respectively; and R is the gas constant.

By keeping the stirring rate at 500 rpm at 30 °C, we changed the concentrations of $[NH_3]$, $[H_2O]$ and [TEOS], respectively, and produced SiO_2 with diameters varying from 172 nm to 806 nm (results shown in Table S1†). Based on these SiO_2 microspheres, corresponding PCs have been prepared. With an increase in the particle size of SiO_2, an obvious red shift in the diffraction peak of the PCs was found (Fig. S1†). The experimental slope (2.27) was in agreement with the theoretic Bragg slope (2.32) from eqn (1). The results shown in Table S2† indicate that these SiO_2 spheres formed close-packed face centered cubic (FCC) structures on the glass slide and the diffraction data from the resulting PCs obeyed the Bragg diffraction law perfectly.

In order to obtain self-reporting MIPCs and achieve visual detection with the naked eye, the λ_{max} values of MIPC films before and after adsorbing the target molecules should be in different areas of the visible spectral region (380–780 nm), that is, $\Delta\lambda_{max}$ should span different color zones upon sensing the target analytes. Mono-dispersed SiO_2 with a particle size of

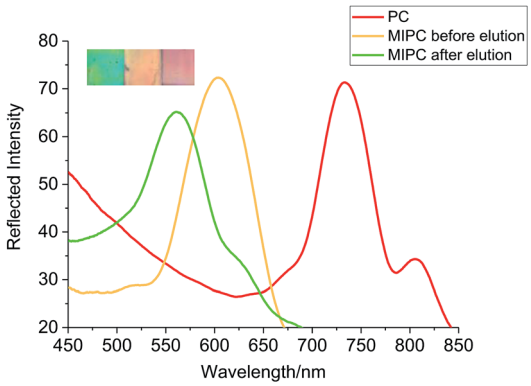

Fig. 2 The diffraction spectra and colors of the PC and inverse opal MIPC (before and after elution).

353 nm was ultimately chosen for the fabrication of the PCs in the present work. The structural color of the produced PCs was red with a λ_{max} value of the diffraction peak of 734 nm (Fig. 2). With the above PCs as a mould, the resulting MIPCs exhibited an orange color with a λ_{max} value of 604 nm before elution of the BZ template. After elution, the λ_{max} value blue-shifted to 561 nm, which is just at the boundary of two color-zones (green and yellow). This provides the premise for obvious color change upon the swelling/contraction of the porous cavities, caused by the binding/elution of BZ.

Whether or not the molecular recognition process can be converted into a readable optical signal depends on the extent of the swelling/contraction of the porous structure of the MIPCs. Optimizing the molar ratio between the template molecule, functional monomers and crosslinkers in the precursor solution is one of the key methods to obtain MIPCs with good elasticity. To achieve optimized polymerization conditions, the effects of the composition of the precursor solution on the analytical performance of the MIPCs were explored. The Bragg diffraction peak shifts of the corresponding MIPCs in response to 10 mM BZ solution were compared, with the results shown in Fig. S2.†

Herein, the imprinted molecule concentration was kept at 0.1 mmol in all precursor solutions (200 μL methanol). The results showed that both the MAA and EDMA content had a great influence on the chemical properties of the MIPCs. As the molecular ratio of MAA was increased from 1 : 2 : 1 (n_{BZ} : n_{MAA} : n_{EDMA}) to 1 : 5 : 1, $\Delta\lambda$ increased from 13 to 18 nm. Upon increasing the ratio of MAA, with $n_{BZ} : n_{MAA} : n_{EDMA}$ ascending to 1 : 8 : 1, $\Delta\lambda$ decreased adversely to 12 nm, due to possible self-combination with excess MAA. Thus, the MAA content was fixed at $n_{BZ} : n_{MAA} = 1 : 5$. Then, the effects of the EDMA content were explored, with the results shown in the inset of Fig. S1.† It was found that when the EDMA content was too low ($n_{BZ} : n_{MAA} : n_{EDMA} = 1 : 5 : 0.5$), the resulting MIPCs were thin and soft. The film easily fell off when the glass slide and PMMA slide were separated, and thus no signal was acquired. Upon increasing the EDMA content until $n_{BZ} : n_{MAA} : n_{EDMA}$ was 1 : 5 : 1.25, a maximum $\Delta\lambda$ value (20 nm) was obtained. However, continually increasing the EDMA content led to the peak shift decreasing gradually. This was because the stronger rigidity of the MIPCs caused by excess crosslinking limited the extent of the swelling/contraction of the cavities, and thus deteriorated the acquisition of optical signals. Based on the above experimental results, a molar ratio of EA/MAA/EDMA of 1 : 5 : 1.25 was used to prepare MIPCs for subsequent experiments.

From the SEM images shown in Fig. 3a and b, it can be proved clearly that both the produced PCs and MIPCs have 3D highly ordered face centred cubic (FCC) structures. The MIPC showed interconnected micropores after removing the BZ molecules and embedded silica microspheres. The sizes of the nanopores of the MIPC seemed smaller than the corresponding SiO_2 particles, due to the contraction of the cavities after removing the embedded silica microspheres. The inverse opal structures of the MIPC are expected to have sufficient surface area, tough mechanical strength, and better sensitivity and optical properties for sensing target analytes.

Sensing properties of the MIPC towards benzocaine

Although conventional molecular imprinting techniques have the ability to result in recognition of target molecules, they lack a direct sensing element. Therefore, the integration of a recognition element with an appropriate transduction element is required. In the present research, an optical response, even a color change, can be generated by the MIPC itself through changes in its 3D-ordered porous structure. Upon analyte adsorption, the porous structure of the MIPC will swell, inducing a red shift in the Bragg diffraction peak. Thus, the molecular recognition process can be directly transferred into a readable optical signal.

In our work, the adsorption efficiency of MIPC films was found to be sensitive to the adsorbing media. In pure water, the response of the MIPC to BZ was found to be poor. However, obvious improvement was achieved with the addition of methanol to the sample medium. The effects of the methanol content on the MIPC diffraction shifts in response to BZ solution (20 mM) are shown in Fig. 4a. As the methanol content increased from 0 to 20%, the $\Delta\lambda_{max}$ value of MIPC diffraction increased from 0 to 35 nm; when the methanol content was over 25%, the $\Delta\lambda_{max}$ value began to drop gradually. Upon continuing to increase the content of methanol to 50%, the $\Delta\lambda_{max}$ value dropped sharply to only 7 nm. The phenomena can be explained as follows: when the water content in the sample solution was high, hydrogen bonding between BZ and the functional

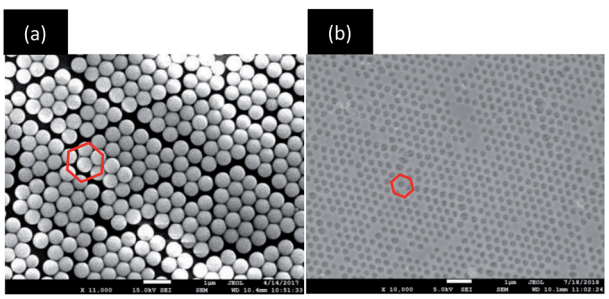

Fig. 3 SEM images of the self-assembled PC and inverse opal MIPC.

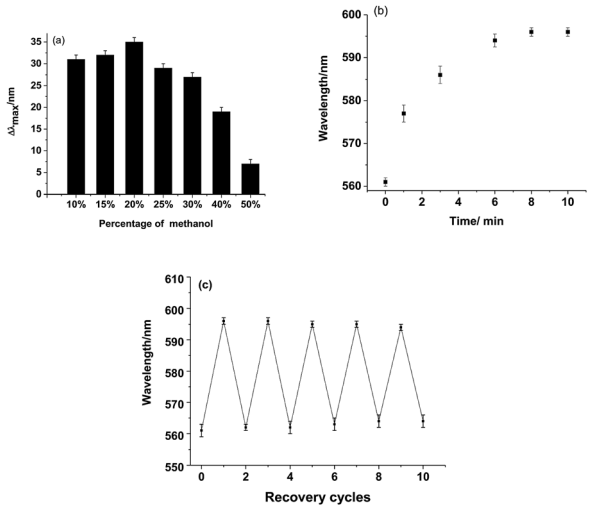

Fig. 4 (a) The effect of the methanol content on the shift of the diffraction peak of the MIPC upon BZ adsorption. (b) The time course of MIPC diffraction upon BZ adsorption. (c) The reversibility of the MIPC in response to BZ.

monomers was destroyed due to the excessive polarity of water, resulting in the low adsorption capacity of MIPC for BZ. Since methanol was used as the porogen in the preparation of the MIPCs, on the other hand, increasing the methanol content in the sample solution was found to be beneficial for the adsorption of template molecules on the MIPC gel. However, when the methanol content was too high, some analytes were dissolved from the gel by methanol instead; thus, the adsorption capacity decreased in this case. In subsequent experiments, the methanol content in the sample solution was controlled at 20% to obtain improved adsorption efficiency. However, for the blank sample, the Bragg diffraction peak did not change at all, whether methanol was added or not. Thus, it was not methanol but the molecular recognition process that caused the red shifts in the Bragg diffraction of the MIPCs.

A quick response is an important requirement for sensors for real applications. The time course of diffraction upon BZ adsorption (20 mM) is shown in Fig. 4b. The diffraction peak red-shifted significantly within 1 min and tended to be stable after 9 min of exposure to BZ. Therefore, a soaking time of 10 minutes was used to obtain a stable signal in this work. The ordered and interconnected macroporous structure of the MIPC endowed the sensor with a rapid response to external stimuli by allowing analytes to diffuse quickly into the hydrogel polymer.

Both the existence of a stable response and the cost effectiveness are determined by whether the sensor can be reused or not. In the present research, the developed MIPC sensor can be easily recovered by elution with a mixture of acetic acid/methanol/water (0.5/3.5/6, v/v/v) to remove the absorbed analytes, owing to the good physical stability of the MIPC. Fig. 4c shows that the MIPC can be regenerated and exhibits a repeatable signal to BZ (20 mM) over five cycles. The RSD between each signal was within 3.04%, which indicates the good reproducibility of the MIPC.

To further investigate the analytical performance of the MIPCs in response to BZ, we inserted MIPC and NIPC films into BZ solutions of different concentrations. The diffraction response of the MIPC film was observed with a fiber optic spectrometer. As shown in Fig. 5a, the optical diffraction shift of the MIPC was sensitive to the rebinding of BZ molecules. The original Bragg diffraction peak wavelength of the MIPC in background solution was 561 nm. With an increase in the concentration of BZ, the MIPC diffraction peak red-shifted gradually and the total red-shift reached about 35 nm, until the BZ concentration was 20 mM. At the same time, the color of the MIPC film changed from green to orange. Fig. 5c shows the linear relationship ($\Delta\lambda_{max} = 1.3724 + 1651.0401C$, $R^2 = 0.9978$) between the $\Delta\lambda_{max}$ value of the MIPC diffraction peak and the concentration of BZ in a range from 0.1 mM to 20 mM. In consideration of possible interference from the sample matrix, the detection limit is regarded as the lowest concentration in the calibration curve, that is 0.1 mM (16.5 μg mL^{-1}).

Differently from the MIPC, as shown in Fig. 5b, the Bragg diffraction of the NIPC changed slightly due to nonspecific adsorption. These results clearly indicate that the microenvironment created by molecular imprinting was responsible for the significant optical signal response of the MIPC. The binding of BZ to the recognition sites of the MIPC actuated an obvious volume increase of micro-cavities, which resulted in the significant red-shift of the diffraction wavelength.

To explore the specificity and selectivity of the developed MIPC/NIPC, we inserted MIPC/NIPC films in benzocaine, ethylparaben, and procaine hydrochloride solution, and 2-hydroxy isobutyric acid, and observed the changes in Bragg diffraction with an optical fiber spectrometer. The structural formulas of benzocaine and its analogues are shown in Fig. 6. The diffraction shifts of the MIPC/NIPC films in different solutions are shown in Fig. 7.

It can be obviously seen that the response of the MIPC to BZ is much higher than to the other analogues. The NIPC cannot discriminate between BZ and ethylparaben, since the structures

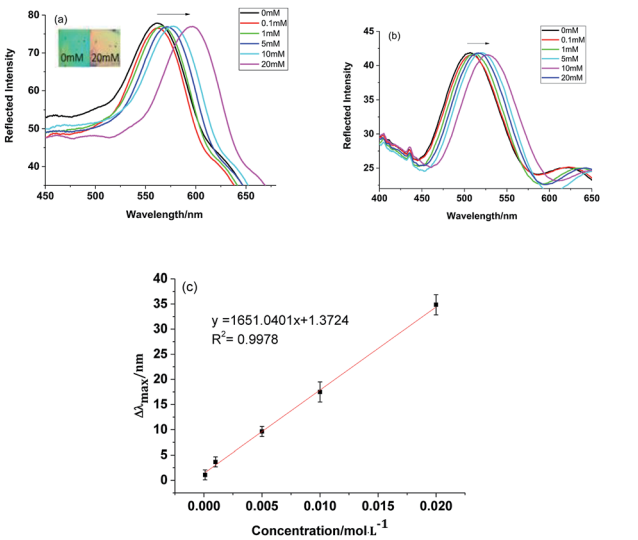

Fig. 5 Diffraction spectra of (a) MIPC and (b) NIPC samples, and (c) a quantitative curve of the MIPC response to BZ.

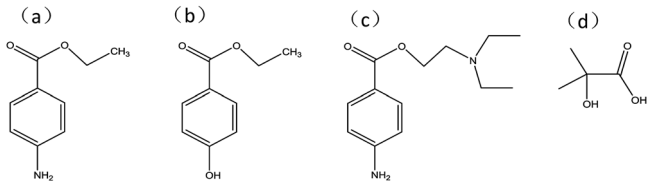

Fig. 6 The structural formulas of (a) benzocaine, (b) ethylparaben, (c) procaine hydrochloride, and (d) 2-hydroxy isobutyric acid.

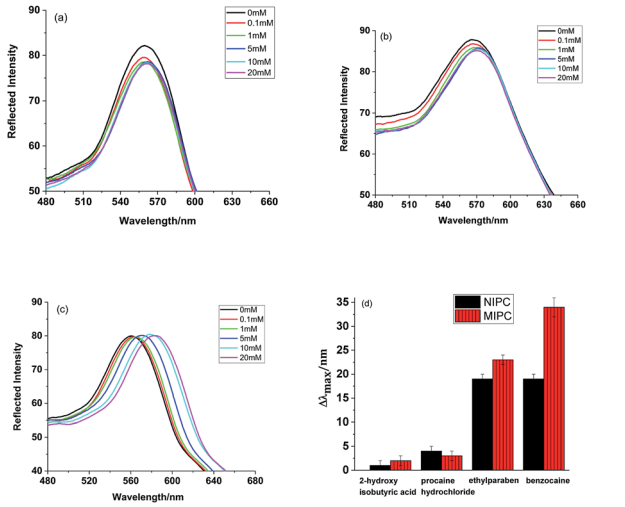

Fig. 7 The diffraction spectra of the MIPC sensor in response to (a) 2-hydroxy isobutyric acid, (b) procaine hydrochloride and (c) ethylparaben. (d) A comparison of the diffraction peak shifts between analogues at 20 mM.

of the two chemicals are too similar. The selectivity and relative selectivity coefficients of the MIPC and NIPC sensors have been calculated. The selectivity coefficient k values for BZ with respect to the selected analogues were obtained from the following equation:

$$k = \Delta\lambda_{max}\,(\mathrm{BZ})/\Delta\lambda_{max}\,(\mathrm{analogues}) \quad (3)$$

where $\Delta\lambda_{max}$ (BZ) and $\Delta\lambda_{max}$ (analogues) are the peak shifts of the sensor in response to BZ and the analogues, respectively.

The relative selectivity coefficient K can indicate the extent of the selectivity enhancement of the MIPC towards BZ with

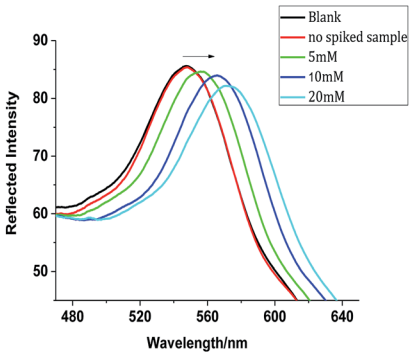

Fig. 8 The diffraction response of the MIPC sensor to fish samples.

respect to the NIPC. It was obtained from the following equation:

$$K = k_{(\mathrm{MIPC})}/k_{(\mathrm{NIPC})} \quad (4)$$

where $k_{(\mathrm{MIPC})}$ and $k_{(\mathrm{NIPC})}$ are the selectivity coefficients of the MIPC and NIPC, respectively.

Based on the results shown in Fig. 7d, the average selectivity coefficient $k_{(\mathrm{MIPC})}$ and $k_{(\mathrm{NIPC})}$ values were calculated to be 9.9 and 4.8, respectively, for BZ with respect to the analogues. Thus, the relative selectivity coefficient K was 2.1, which means that the selectivity of the MIPC was 2.1 times that of the NIPC with regards to the selected analogues. The results showed that the MIPC possessed better recognition ability toward BZ than the other three analogues. Therefore, apart from offering remarkable sensing characteristics surpassing the NIPC, the MIPC can delicately distinguish the differences between BZ and other analogue molecules. The specific molecular recognition behavior of the MIPC mainly depends on two factors: the molecular dimensions of the analytes and the matching degree to the binding sites. With its complementary shape, size and functional group arrangement in relation to the formed binding sites, only BZ, rather than the other analogue molecules, can specifically occupy the imprinted cavities within the MIPC film and cause an obvious volume change in the hydrogel film, resulting in the significant shift of the Bragg diffraction peak.

Application to food detection

Under the optimized conditions, the MIPC sensor was applied to analyze BZ in fish samples. To investigate the test accuracy of the presented method, a comparison between the MIPC and

Table 1 A comparison between HPLC and MIPC methods for the detection of BZ in fish samples ($n = 3$)

	Measured concentration (mM)		Recovery rate (%)		Average of recovery rates (%)	
Added concentration (mM)	MIPC	HPLC	MIPC	HPLC	MIPC	HPLC
5	4.43	4.34	88.60	86.80	86.65	87.57
10	10.34	10.66	103.40	106.60		
20	13.59	13.86	67.95	69.30		

HPLC methods was performed. Since no residues of BZ were found in all samples using both methods, fish samples were spiked with BZ at different concentrations. For each concentration level, three replicate experiments were performed, with the results shown in Table 1 and Fig. 8. The mean recovery of BZ with the two methods was found to be in good agreement. For BZ at lower concentrations, the recovery values of the developed method and HPLC method varied from 88.60–103.40% and 86.80–106.60%, respectively. For BZ at high concentrations (20 mM) in fish samples, both methods showed lower recovery values. These results indicate that both methods are not suitable for detecting BZ at high concentrations in real samples due to possible interactions or aggregation of BZ in complicated sample matrices. For high concentrations of BZ, samples must be diluted before analysis. The relative standard deviation (RSD) values between the two methods are below 0.60%. Through comparison with HPLC, the recovery rates using the MIPC are considered to be acceptable and can be extended to the routine analysis of trace BZ in real samples.

Conclusions

In this article, we developed a novel "smart" sensor based on a combination of photonic crystal and molecular imprinting techniques for the convenient and visual detection of benzocaine. Benefiting from the highly ordered hierarchical structure of photonic crystals and the specificity of molecularly imprinted polymers, the smart sensor can directly transfer the molecular recognition process into a readable signal. With many advantages, such as high sensitivity and specificity, quick response times, good regeneration abilities, direct transduction and label-free measurement, the sensing system has great potential for on-site screening and the visual detection of trace BZ in real samples. For real sample applications, the developed method has shown good reproducibility and satisfactory accuracy in comparison with HPLC methods. After further optimization, such sensors can hopefully be applicable to the real-time visual detection of drugs, diseases, and pollution in various food-related and environmental areas.

Conflicts of interest

There are no conflicts to declare.

Acknowledgements

This work was supported by the National Natural Science Foundation (21477026, 21677053, 21876033), the Science and Technology Program of Guangzhou (201607010295), the Postgraduate "basic innovation" Project of Guangzhou University (2017GDJC-M09), the Undergraduate "innovation training" Project of Guangzhou University (201711078061), and the 2018 "Challenge cup" Project of Guangzhou university.

References

1 T. S. Hori, A. K. Gamperl, L. OB Afonso, S. C. Johnson, S. Hubert, J. Kimball, S. Bowman and M. L Rise, *BMC Genomics*, 2010, **11**, 72–94.
2 X. H. Chen, Y. J. Zhu, J. Y. Liu, D. G. Yang, H. Du and Q. W. Wei, *Freshw. Fish.*, 2006, **36**, 39–42.
3 L. L. Marking and F. P. Meyer, *Fisheries*, 1985, **10**, 2–5.
4 Y. F. Li, *Shaanxi Journal of Agricultural Sciences*, 2015, **61**, 66–67.
5 H. Danafar, M. Hamidi and T. C. Hsu, *Cogent Med.*, 2016, **3**, 1129790–1129801.
6 H. S. Amr, A. A. G. Medhat, A. G. A. Sohair and M. L. Hayam, *Food Chem.*, 2016, **190**, 982–989.
7 Y. B. Lu, Z. Cheng, C. Liu and X. Cao, *Food Anal. Method*, 2016, **9**, 1857–1866.
8 F. Giusti, G. Caprioli, M. Ricciutelli, S. Vittori and G. Sagratini, *Food Chem.*, 2017, **221**, 689–697.
9 X. J. Sun, Y. H. Yang, Q. B. Tian, D. R. Shang, J. Xing and Y. X. Zhai, *J. Chromatogr. B: Anal. Technol. Biomed. Life Sci.*, 2018, **1093**, 167–173.
10 M. Mohammadnejad, T. Hajiashrafi and R. Rashnavadi, *J. Porous Mater.*, 2018, **25**, 1771–1781.
11 S. Yang, K. Kwon, J. Choi and C. H. Jo, *Food Sci. Biotechnol.*, 2018, **27**, 859–866.
12 F. J. Lara, D. Airado-Rodríguez, D. Moreno-González, J. F. Huertas-Pérez and A. M. García-Campaña, *Anal. Chim. Acta*, 2016, **913**, 22–40.
13 M. A. O. Mei, A. A. Elbashir and O. J. Schmitz, *Food Chem.*, 2017, **214**, 300–307.
14 T. T. Xiao, X. Z. Shi, H. F. Jiao, A. L. Sun, H. Ding, R. R. Zhang, D. D. Pan, D. X. Li and J. Chen, *Biosens. Bioelectron.*, 2016, **75**, 34–40.
15 E. Yablonovitch, *Phys. Rev. Lett.*, 1987, **58**, 2059–2062.
16 D. H. Ge, J. H. Zhang, L. Q. Zhang, L. Lu and X. K. Huang, *Mater. Sci. Eng.*, 2017, **170**, 012005.
17 X. Zhou, M. Z. Li, W. Kang, H. Z. Li, Y. A. Li, C. Li, Y. L. Yan, Y. S. Zhao and Y. L. Song, *ChemPhysChem*, 2018, **19**, 2101–2106.
18 Q. P. Kong, B. B. Xie, S. Preis, Y. Hu and H. Z. Wu, *RSC Adv.*, 2018, **8**, 8950–8960.
19 J. P. Lai, Y. Zuo, H. Sun and Y. Yu, *RSC Adv.*, 2015, **63**, 51392–51398.
20 D. Capoferri, R. Álvarez-Diduk, M. Del Carlo, D. Compagnone and A. Merkoçi, *Anal. Chem.*, 2018, **90**, 5850–5856.
21 S. Je Cho, H. B. Noh, M. S. Won, C. H. Cho, K. B. Kim and Y. B. Shim, *Biosens. Bioelectron.*, 2018, **99**, 471–478.
22 Y. L. Li, H. Sun, J. P. Lai, X. Y. Chang, P. Zhang and S. L. Chen, *Microchim. Acta*, 2018, **185**, 122–133.
23 S. A. Zaidi, *RSC Adv.*, 2016, **91**, 88807–88819.
24 J. Zhang, J. Liu, Y. Zhang, F. Yu, F. Wang, Z. C. Peng and Y. C. Li, *Microchim. Acta*, 2018, **185**, 78–85.
25 A. El-Beqqali, L. I. Andersson, A. D. Jeppsso and A. R. Mohamed, *J. Chromatogr. B: Anal. Technol. Biomed. Life Sci.*, 2017, **1063**, 130–135.

26 H. Sun, J. P. Lai, F. Chen and D. R. Zhu, *Anal. Bioanal. Chem.*, 2015, **407**, 1745–1752.
27 W. Lu, S. A. Asher, Z.-H. Meng, Z. Q. Yan, M. Xue, L. L. Qiu and D. Yi, *J. Hazard. Mater.*, 2016, **316**, 87–93.
28 N. Sai, Y. T. Wu, G. G. Yu, Z. Sun and G. W. Huang, *Talanta*, 2016, **161**, 1–7.
29 X. H. Zhang, Y. G. Cui, J. L. Bai, Z. Y. Sun, B. A. Ning, S. Li, J. Wang, Y. Peng and Z. X. Gao, *ACS Sens.*, 2017, **2**, 1013–1019.
30 J. J. Dai, D. Vu, S. Nagel, C. H. Lin and M. F. De Cortalezzi, *Microchim. Acta*, 2018, **185**, 32–38.
31 C. J. Xiong, J. P. Zhao, L. B. Wang, H. B. Geng, H. B. Xu and Y. Li, *Mater. Horiz.*, 2017, **4**, 862–868.
32 H. Choloong, O. Cha-Hwan and H. Wang, *J. Korean Phys. Soc.*, 2011, **58**, 1116–1119.
33 A. Richel, N. Johnson and D. W. McComb, *Appl. Phys. Lett.*, 2000, **76**, 1816–1818.
34 N. P. Johnson, D. W. Mccomb, A. Richel, B. M. Treble and R. M. De La Rue, *Synth. Met.*, 2010, **116**, 469–473.
35 T. A. Ukleev, N. N. Shevchenko, D. I. Iurasova and A. V. Sel'kin, *Phys. Solid State*, 2018, **60**, 916–920.
36 R.-Y. Zhao, P. Dong and W.-J. Liang, *Acta Phys.-Chim. Sin.*, 1995, **11**, 612–616.